Diagnosing and Online Partial Discharge Location with Using Coupling Capacitor in Induction Motors

Seyed Mahdi Mazlomi[1] and Seyed Mohammad Hassan Hosseini[1,*]

ARTICLE INFO

Article history:
Received: 30 November 2021
Revised: 24 January 2022
Accepted: 29 April 2022

Keywords:
Partial discharge
Induction motors
PD online measurement

ABSTRACT

Induction motors must have partial discharge measurements to prevent an electric breakdown. In this study, coupling capacitors of different capacities were used to measure online partial discharge in invertor-fed rotary induction motors without filters at the inverter's output. In addition, high-frequency variants of cables and machinery are used. Partial discharge causes insulation degradation to worsen over time and, in the worst-case scenario, result in a complete loss. This is precisely what needs to be prevented. This is accomplished through the partial discharge test. It aids in the early detection of potential future complete failures. The position of the partial discharge (PD) on the stator winding of an induction motor is proposed in this study in three different ways: modeling the partial discharge's source, modeling its course, and modeling its monitoring system. The suggested model's three-phase motor winding, partial discharge source, and measurement circuit are all simulated using the Matlab-Simulink environment. Additionally, modeling at three locations vulnerable to partial discharge is used to confirm the viability of the suggested technique.

1. INTRODUCTION

Partial discharges are without a doubt the primary cause of insulation failure in high voltage motors and transformers, which degrades the insulator over time and eventually causes its entire destruction. Consequently, identification and diagnosis of this phenomenon's effective variables are crucial for investigating and controlling the insulating equipment's safety. According to IEC60270, partial discharge is often accompanied by sound, light, heat, and chemical reactions. Consequently, various methods are used to analyze partial discharge behavior based on electrical measuring instruments, including traditional electrical measurements in the narrowband-wideband frequency domain, audio measurements (10 -300 kHz), high-frequency optical, chemical, and electrical measurements comprising the VHF method (10-300 MHz) and the UHF method (300 MHz- 3 GHz) [1-4]. In reference to online PD-Cable monitoring systems, a new partial discharge technique (PD) based on PD pulse Rise-Time and Transfer-Function (RTTF) has been studied in [5]. This approach is based on rising time alterations that are dependent on the length of the cable through which the PD pulse has been transmitted. In [6], pure RF received signal characteristics of PD pulse are employed to inexpensively find online PD. On the premise that PDs create distinctive RF spatial patterns owing to the complexity and nonlinearities of RF propagation, a localization technique based on the study of these characteristics has been devised. In this method, two unique frequency bands with distinct PD data are used. From the primary PD signal and the two sub band signals, PD location characteristics are derived. In reference to the mechanism, PD propagation of PD pulse in the stator winding, PD signal detection methods, and signal processing techniques, [7] provides detailed research. The measurement of partial discharges using an antenna sensor has been studied in [8]. The sensor's absence of disturbance is one of its most crucial characteristics. The frequency response of the antenna source to automatically distinguish various PD sources and synchronize them with the supply voltage has been detailed and examined in depth. Using electromagnetic waves, [9] presents an experimental investigation on the eradication of partial discharge and detection of radial deformation of high voltage transformer winding. Researchers are interested in the online identification of problems in power transformers owing to their technological and economic benefits.

Recently, the high-frequency synthetic aperture radar approach for detecting radial deformation has been explored. In this work, a monitoring system is constructed and tested on an actual transformer winding utilizing the aforementioned techniques to identify these defects. A novel method for precise replacement of partial discharge in an oil insulation system is presented in [10]. The

[1]*Electrical Engineering Department, South Tehran Branch, Islamic Azad University, Tehran, Iran.*
**Corresponding author:* Seyed Mohammad Hassan Hosseini; E-mail: smhh110@azad.ac.ir.

objective of the research was to identify dynamics and noise measurement series in a PD replacement system and utilize this data to improve the estimation of an extended Kalman-Filter (EKF) and predict the position of PD. Using the UHF approach, [11] presents theoretical research on the partial discharge source localization in high voltage transformers. In addition, a short overview of common PD sources, a continuous UHF-based monitoring system, and relevant UHF sensor types are provided. Using an ultrasonic detection system contained in a 2*2 optical fiber Fabry-Pérot sensor array with a direct response algorithm as described in [12], partial discharge replacement in transformer oil is performed. In [13], a technique for detecting dispersed partial discharges and evaluating the voltage resistance of high voltage cables is provided. Distributed partial discharge detection employs a frequency-selected current, an optical cable, and 3G technology to accomplish simultaneous monitoring of the PD signal. A distributed system for the detection and localization of partial discharges in substations is described in [14]. The suggested system consists of multiple distributed UHF antennas that form an array. In [15], a diffusion drift model is utilized to simulate single discharge within a spherical air-filled atmospheric pressure using proxy resin. Utilizing a diffusion drift model, PDs between spherical electrodes covered with dielectric materials are studied. The model geometry is an axisymmetric analog of crossed wire studies used [16] to explore PD activity caused by impulsive voltage waveforms. The coil is utilized to detect partial discharge in the 3.3 kV motor in [17].

Due to the problem of noise, the majority of investigations identify PD at the power or neutral bus. To detect PD, we place three coils into the slots of three motor frames. In [18], a unique approach for identifying capacitor faults is described. Using an artificial neural network algorithm (ENN) and chaotic synchronization detection technique, the problem in the power capacitor is detected using this approach. Partial discharge was monitored using hardware circuits such as a high-frequency current transformer (HFCT), high-pass filter, noninverting amplifier circuit, and high-frequency oscillography for signal collection. Electrode simulation for PD location modeling in an oil-insulated power transformer and the implementation of the acoustic emission (AE) approach are presented in [19]. The objective of this design is to simulate a basic PD signal in order to save time during the experiment. The design must account for the PD-causing electric field stress at the electrodes (anode). The precise determination of the location of a partial discharge in an oil insulation system has been addressed in [20]. This model presents a mechanism for compensating for increasing noise statics caused by sensor aging or external noise. A strategy for partial discharge replacement based on an ultrasonic sensor array with a double helix has been suggested in [21]. A low-cost method for continuous monitoring of PD employing inexpensive radio sensor networks for sampling of position patterns of received power signal has been described in [22]. In [23], ultra-high frequency and acoustic emission in partial discharge diagnostic techniques and diagnosis of decomposition gas SF6 are described, and in each instance, frequent partial discharge problems of GIS equipment are introduced by different diagnosis methods. A passive radio frequency (RF) sensor for non-invasive radiometric diagnosis of simultaneous partial discharge (PD) signals in high-voltage (HV) equipment has been reported in [24]. The sensor is a passive circuit comprised of many resonators and an antenna for collecting PD signals.

Single-pulse analysis with partial discharge replacement was presented in [25]. Since it is seen that PD drops during propagation, the proposed approach allows us to segregate PD pulses in various portions of generator coils. A very sensitive measuring antenna is inserted within the test item or situated near to the test object to accomplish the partial discharge measurement at an open stator winding. An antenna cannot be used to measure at a fully constructed motor because the closed motor cabinet shields the high-frequency emissions. These measurements are made using a unique coupler that is coupled to the measuring lead. This is in part owing to the complicated mechanism of PDs and the propagation characteristics of PDs in stator windings, which make it challenging to find an appropriate detection site and sensor. In addition to signal misinterpretation due to harmful noise and disturbances on-site, which may be more frequent and of greater amplitude than the PD signals. In addition, the simultaneous occurrence of several PD sources makes it difficult to distinguish distinct PD sources. Theoretical estimations and experimental observations suggest that the frequency spectrum of a rapid rise-time unipolar PD pulse comprises signals ranging from DC to GHz signals. In an attempt to increase the sensitivity of PD measures, tremendous strides have been achieved in online PD assessment over the last several decades, and a variety of on-site approaches have been developed and used.

Epoxy-mica insulated capacitors are extensively utilized nowadays as a result of the advancement of production processes. Neutral Capacitor Coupling (NCC) inherits the great dependability of Neutral RFCT Coupling (NCT) and outperforms it in terms of sensitivity. NCC's detecting frequency range was comparable to that of NCT. Low signal-to-noise ratio (SNR) presents an insurmountable obstacle to PD signal interpretation and subsequent insulation condition evaluation. HV Terminal Capacitor Coupling (HVCC) is the off-line test method defined by substituting the huge coupling capacitor with a much smaller one of around 80 pF linked with a resistive detecting impedance; this system was the ancestor of the following PD analyzer (PDA), i.e. HVCC. Differential and

directional modes are included in PDA. Exists an internal circuit ring of suitable length. Installing one coupling capacitor per line end of each parallel helps to isolate PD from noise generated by an external generator based on arrival time and pulse patterns. At the output bus per phase, two coupling capacitors are provided, one as near as feasible to the terminal and the other at least 2 m distant toward the transformer. The directional PDA employed delay lines and a balanced PD detecting circuit to distinguish between external noise and internal PD. A typical PDA capacitor is an 80-pF epoxy-mica capacitor with a detection frequency range of 40 MHz350 MHz and a high SNR with respect to a minimal number of windings. According to one provider, these capacitors can only monitor around 5% of the bars of each phase near the HV terminal. Capacitors with greater capacitance can detect more PD energy, making them more sensitive to PD deep in the stator winding.

2. ELECTRICAL DIAGNOSIS METHODS OF THE PARTIAL DISCHARGE

The most effective approaches for electrical partial discharge diagnostics are partial discharge pulses. In the diagnosis of partial discharges, the transformed reactive load between the insulating system's terminals is an appropriate physical quantity. There are a number of circuits to diagnose partial discharge based on pulses current diagnostic brought on by partial discharge, but generally speaking, the fundamental circuit is shown in Figure 1.

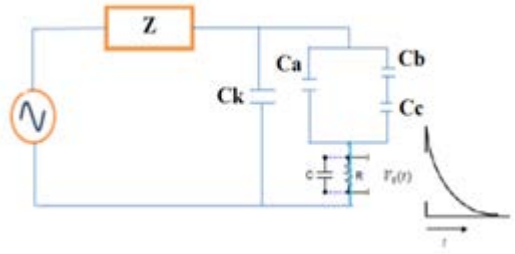

Fig. 1. The base circuit of partial discharge diagnosis.

This circuit's components are: (1) a high-voltage source that is free from partial discharge; (2) a high-voltage source impedance (Z); (3) a test insulation where partial discharge occurs (the well-known a-b-c model); (4) a coupling capacitor Ck; and (5) an impedance (Zm) through which partial discharge-based current pulses in the test isolator pass. 6) An amplifier; seven) An oscilloscope.

2.1 Voltage drop method of insulator terminals

For the purposes of this approach, a cavity in a solid or liquid sample isolator is equal to a simple capacitor. Due to the difference in the dielectric coefficient, a gas-filled cavity—typically air—would be the source of partial discharge if an increase in the applied voltage across A-B terminals resulted to a noticeably higher gradient of a voltage across the cavity. The initial discharge for continuous voltage happens in the positive half-cycle, greatly depleting Cc, and starting a discharge current flow. Due to the semi-impulse nature of this current's nanosecond pulse, it cannot be monitored right away [19]. Assuming that voltage V for isolator and voltage zero for A and B terminals, by closing the switch S, electrical charge $q_c = C_c \delta V_c$ will release which is a loss charge in the system. Voltage drops on terminals δV_a simply is calculated by comparing system charge before and after this discharge [19]:

$$\delta V_a = \frac{C_b}{C_a + C_b} \delta V_c \quad (1)$$

Although, voltage drop inside the cavity δV_c is relatively high because $\frac{C_b}{C_a + C_b}$, $C_a \gg C_b \gg C_c$ often is very small, the voltage drops δV_a is smaller. As a result of using a direct detecting method, calculating this step voltage by measuring the input voltage method would be futile. Therefore, using the detection circuits to measure other suitable quantities seems necessary [20].

2.2 Detection impedance

Essential for diagnosing partial discharge-based current pulses in the sample isolator is the use of a detecting impedance. The voltage drop caused by partial discharge current flow is proportional to the integral of the current or apparent load transmitted between the test insulator's terminals. The amplification and processing of this voltage, whose amplitude is related to the transferred apparent load, give vital information on the insulation's state in terms of the intensity and kind of partial discharges [21]. Figure 2 depicts the many types of detecting impedance.

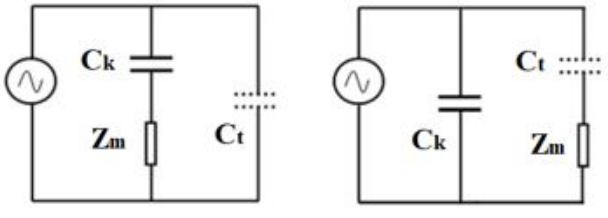

(b) **(a)**

Fig. 2. Detection impedance with sample resistance (a)- impedance in series with coupling capacitor (b)- impedance in series with sample insulator.

There are generally two methods to add this impedance to the detector circuit. Impedance in series with the coupling capacitor is (a). impedance connected in series to the sample regulator (b). Both architectural designs for the distribution capacitor are electrically identical, but the polarity of the current flow based on partial discharge is different. Naturally, the high voltage source's impedance

must also be sufficient to provide the necessary current for partial discharges from the coupling capacitor alone. In actuality, however, measuring impedance in series with the regulator would be more accurate. The primary drawback of this approach is that if the sample resistor is completely discharged, the circuit will be damaged. However, the design with the coupling capacitor and impedance in series does not experience serious current flow problems. It should be noted that some of the partial discharge-based current will travel through the distributed capacitors between the high-pressure bus and ground and not all of it will go through the sampling resistor [21].

2.3-RC detector impedance

The simplest detector impedance form Zm is a single resistor, but since the existence of dispersed capacitors is unavoidable, its simplest form in practice is regarded to be an RC circuit. Using the impulse current caused by the partial discharge as input and the voltage across both ends as the output of this impedance, the Laplace transform can be used to calculate the impedance of Fig. 1 according to Eqs. (2) and (3):

$$V_0(t) = \frac{q}{C_a + C\left(1+\frac{C_a}{C_k}\right)} e^{-\left(\frac{1}{2RC_c}\right)t} \quad (2)$$

$$C_a = \frac{C_a.C_k}{C_a+C_k} + C \quad (3)$$

where, q is an apparent transformed charge among the terminals of the insulator in terms of discharge:

$$q = C_b \delta V_c \quad (4)$$

The output amplitude of this circuit is proportional to apparent load q, as shown by the response of the RC circuit to an impulse brought on by the transformed apparent load q. RC stands for the reaction time constant. The output response will be crisper and the time constant will be less with a smaller resistance R. Because an amplifier cannot completely amplify this rapid pulse, its harmonics will be muted. The response's amplitude will not be impacted by resistance R. It should be noted that this RC circuit may be regarded as a filter for frequencies greater than f = 1 / (2 πRCc) [22]. It would be challenging to reliably differentiate between neighboring pulses since a long-time constant lead to intractable inference problems. Without a coupling capacitor, C/Ck approaches to infinity, which causes the pulse's size to be astonishingly tiny. As a result, it will be quite difficult to detect it, making coupling capacitor Ck an essential part of this circuit [19].

2.4 RLC detector impedance

By exhibiting low impedance to low-frequency currents, a parallel inductor to the RC detection impedance will filter low frequencies of the output signal, such as the sine voltage frequencies of the voltage source. Due to oscillation and inference issues, the Q-factor of the chosen RLC circuit must be as low as feasible [19]. Using the Laplace transform, the response of the detector impedance for the RLC circuit may also be computed. The results of the RLC detector computations are stated in Eq. (5) and Eq. (8):

$$V_0 t = \frac{q}{C_a + C\left(1+\frac{C_a}{C_k}\right)} e^{-\left(\frac{1}{2C_c}\right)t} \quad (5)$$

$$w = \left(\sqrt{\frac{1}{LC_c} - \frac{1}{4R^2.C_c^2}}\right) = w_0\sqrt{1 - a^2 LC_c} \quad (6)$$

$$a = \frac{1}{2R_c} \quad w_0 = \frac{1}{\sqrt{LC_c}} \quad (7)$$

$$Q = \frac{w_0}{2a} = \frac{R}{\sqrt{\frac{L}{C_c}}} \quad (8)$$

where, C_a is obtained from Eq. (3) and q is obtained from Eq. (4).

As with the RC circuit, the output voltage amplitude is seen to be proportional to the apparent load q and the resistance R, with no influence on the response amplitude. The damping time of the oscillations is essential due to pulse overlap concerns. The RL circuit's quality factor decreases as the damping time becomes shorter. Typically, damping may be done with a Q = 1.

3. PD REPLACEMENT AND RECOGNITION METHODS AND MECHANISM OF PD PULSES MOVEMENT

Those who have performed PD measurements on a motor or generator are well aware that the results are typically derived from two or more PD sources. In order to make a reliable assessment of the risk posed by the individual phenomena, it is crucial to distinguish these individual PD sources. There are two primary methods for recognizing partial discharges in windings, based on time domain and frequency domain algorithms. Included in time-domain algorithms are peak detection, 50% peak detection, 20% peak detection, the Akaike information criterion, correlation, the energy criterion, and the Gabor criterion. Recently proposed frequency domain algorithms are based on the phase difference measurement method [23]. To minimize signal interference as much as possible, it is possible to digitize the signals at the point of acquisition. No longer are analog signals transmitted over long distances, making the measurement as robust and reliable as possible. Frequency-selective measuring systems also permit the selection of various filter settings and measurement at much lower noise levels at higher frequencies. In winding, time-based partial discharge replacement methods can be measured from either two or one ends. These techniques are known as two-end and one-end location systems, respectively. This method is referred to as time domain reflectometry.

3.1 Two-end partial discharge replacement system

Two identical signals are produced by a partial discharge that is created at a distance from the first end of the winding. While another wave is transmitted in the opposite direction to the other end of the winding, one of these waves propagates to the first side along the winding at a certain speed. These two waves will arrive at the winding at separate times if they travel different lengths down the winding. High-pressure devices are used to measure, receive, and store these waveforms on both ends of the winding [24].

3.2 One-end partial discharge replacement system

Figure 3 depicts a straightforward view of a winding's one-end partial discharge measuring system. The measuring tool is at one end of this system.

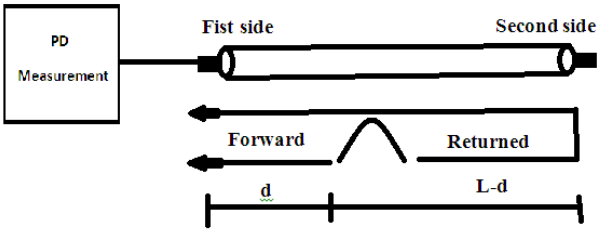

Fig. 3. Schematic of a partial discharge measurement system on one end (left).

Two signals are generated when a partial discharge occurs at a distance d from the end being monitored. While the second signal travels to the opposite side of the winding, the first signal is conveyed with a particular propagation speed to the first end, where the measuring instrument is situated. The collision causes the second signal to be reflected and transmitted back to the first end when it reaches the opposite side of the winding. The direct signal and the reflected signal are the first and second signals, respectively, to arrive to the measuring device [23].

4. MODELING AND FORMULATION OF THE PROPOSED METHOD

4.1. PD Source Modeling

1) Several models may be used to simulate the partial discharge pulse. The two models that are briefly explained are the most prevalent ones: The Gaussian model [10] and the double-exponential function model.

Gaussian model: Figure 4 indicates PD source pulse as a Gaussian function in time and frequency domain. In the Gaussian model, the PD pulse source is modelled in the form of Eq. (9):

$$I(t) = I_0 \tag{9}$$

where, I_0 is the peak current pulse and the pulse width is equal to $2.36\,\sigma$.

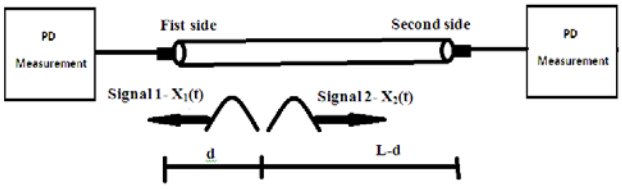

Fig. 4. PD source pulse as a Gaussian function in time and frequency domain.

The magnitude of the pulse is computed as Eq. (10):

$$Q = \int I(t)\,dt = I_0\sigma\sqrt{2\pi} \tag{10}$$

In this equation, the pulse magnitude is due to Coulomb (c).

The Fourier transform of a Gaussian function is expressed as Eq. (11):

$$I(\omega) = Q\exp\left(-\frac{1}{2}\omega^2\sigma^2\right) \tag{11}$$

2) Fig. (4) displays the PD source in three different forms—1, 2, and 3—in the time and frequency domain. The time domain pulse shapes are shown in the first column. The pulses' amplitudes are all 10 A, and their respective rise times are 2 ns, 20 ns, and 360 ns. The frequency domain of PD signals is represented in the second column.

Double-exponential function model: A PD pulse in the time domain can be defined with double exponential functions as Eq. (12).

Eq. (13) is the Fourier transform form of this equation:

$$V(t) = V_0(-e^{(-t/\tau_1)} + e^{(-t/\tau_2)}) \tag{12}$$

$$V(f) = \frac{1}{\tau_2-\tau_1}\left(-\frac{1}{j2\pi f-1/\tau_1} - \frac{1}{j2\pi f-1/\tau_2}\right) \tag{13}$$

where, the constant τ_1 indicates the rise time and the constant τ_2 indicates the fall time.

Figures 5 and 6 display the PD source as Gaussian and double-exponential functions in the time and frequency domains, respectively. The topic of the first column is the form of the time-domain pulses. The pulses have the same 10 A amplitude in all three forms. The rise times are 2 ns, 20 ns, and 360 ns, respectively, while the drop times are 150 ns, 2 ns, and 3 ns. The frequency domain of PD signals is shown in the second column.

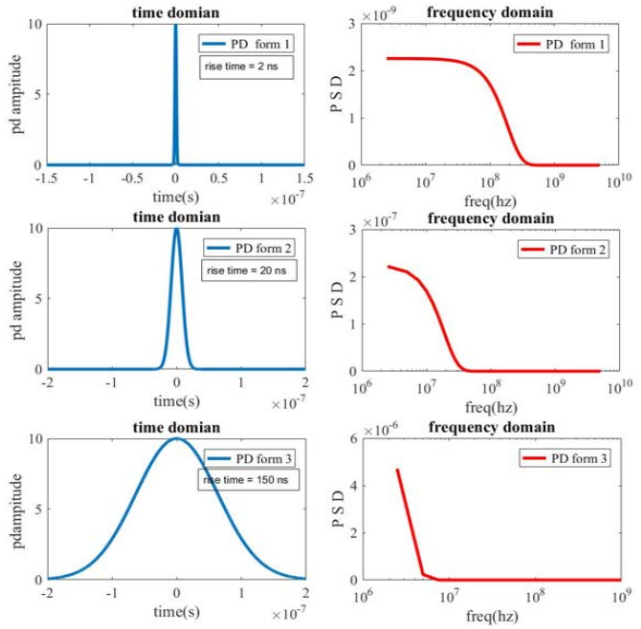

Fig. 5. PD source pulse as a Gaussian function in the time and frequency domain.

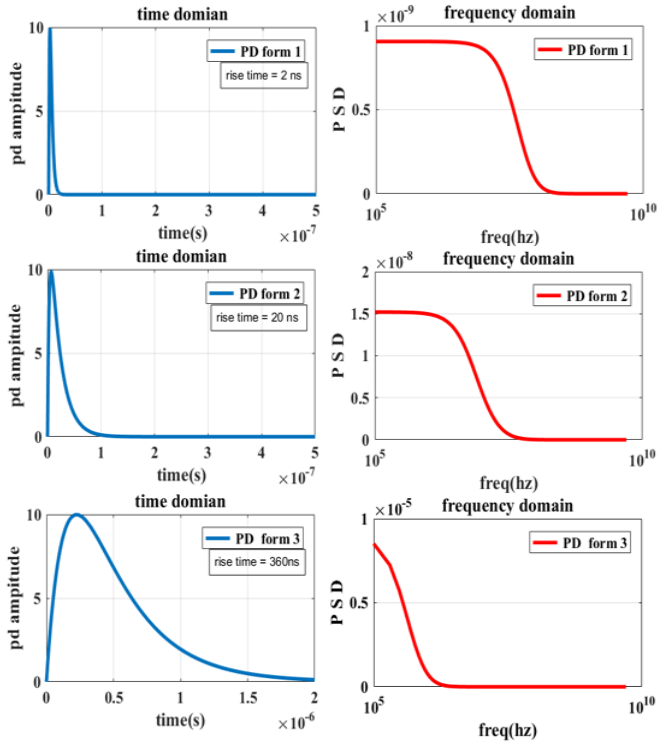

Fig. 6. PD source pulse as a double-exponential function in the time and frequency domain.

4.2 Modeling of motor winding modeling

As the original PD signal moves from the PD source to the measurement terminals, it deforms and dampens (bushing). A signal transmission function may be used to characterize the PD signal waveform. An RLCM circuit that represents the winding and motor insulation system may mimic a PD signal transmission function in the first order. R stands for resistor, L for inductance, C for capacitor, and M for cross-inductance. The response of this RLCM circuit is shown by the measured time of the PD recorded signal at the motor terminals (or higher-order models).In this paper, the ladder model is used to simulate the entire motor winding, including the coils and loops. Coupling between the phases is omitted because the PD signal phase in some locations is lower than the PD source's peak phase. Each rung or component of the ladder is a coil of winding in the ladder model.

4.3 Single-loop winding model

Z1 and Z2 are the invisible and visible portions of the coil, respectively, in a single loop of the motor winding. Z1 and Z2 are made up of four components. Rs is the motor coil's series resistance expressed as a function of length. Ls1 stands for the insulator's inductance per unit length of the coil inside the slot, while Ls2 refers to the insider's inductance per unit length in the coil's outer area. The resistance of the coil within the gap and the outside portions of the coil in relation to the ground are the parallel resistances RP1 and RP2, respectively. The inside coil's capacity is CP1, whereas the outside coil's capacity is CP2.

4.4- Coil transmission line model

The motor's series coils are low-profile, long rings. The model parameters for the winding analysis utilizing the transmission line model are displayed in Figure 7. The series coil's inductance is given by L, the line series resistance is given by R, the coupling capacitor between the coil and the ground is given by C, and the coupling capacitor between the coils is given by K. The circuit above may be expanded as shown in Figure 8 for N coils.

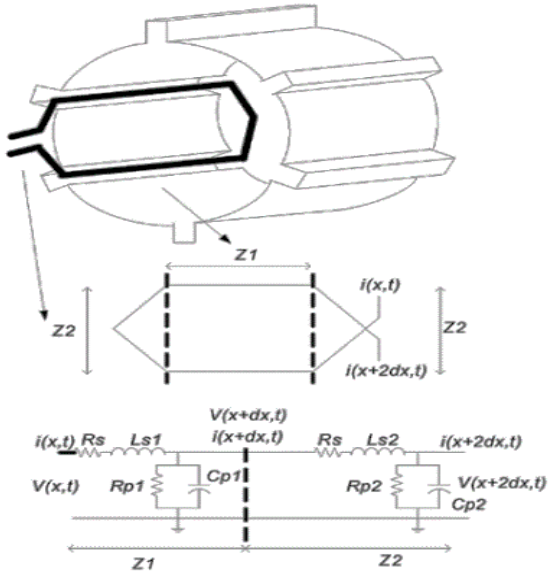

Fig. 7. Transmission line model for motor winding.

Table 1: Parameters of induction motor

Parameter	Power (kW)	Phase voltage (v)	Frequency (Hz)	Pole	Rotor/Stator slots
Value	3.7	380	50	8	44/48

Table 2: The parameters used in the simulation

Parameter	Value
C_{2S}	3.8 nF/section
C_{1S}	0.75 nF/section
L_S	55 nH/section
R_S	80 mΩ/section

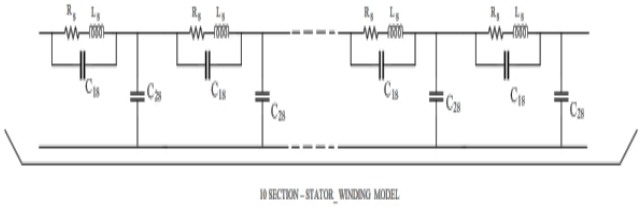

Fig. 8. Motor stator winding model circuit for N single phase coil.

This study aims to identify the PD in the induction motor's stator winding. Three phases are used to represent the issue:

1) Partial discharge source modelling (applying double-exponential model partial discharge source is modelled as a current source)

2) Modeling the partial discharge propagation path (motor windings are propagation path and modelled using proposed model (ladder model) in which every coil is modelled as a ladder step with four parameters)

3) Modeling of the partial discharge measurement system (measurement system involves a coupling capacitor and a 50 0hm resistor).

5. SIMULATION AND ANALYSIS OF RESULTS

A partial discharge source, a three-phase motor winding with ten coils per phase, and a measurement circuit (coupling capacitor) are all included in the conceptual model and are all simulated as 3-dimensional models using the MATLAB Simulink tool. A, B, and C represent three potential places for a partial discharge in each phase. Three kinds of simulation for phase R were used (PD pulse injection at point A, PD pulse injection at point B, PD pulse injection at point C). Simulated results are applied to all three stages, although just one phase is simulated for the sake of simplicity. IEC-60270 states that partial discharge (PD) happens as a result of electrical stress on the insulation, which makes high voltage portions of the motor winding susceptible to PD. Each coil in this article is modeled as a ladder, and each motor phase includes 10 series coils. The last three coils, which are more prone to PD incidence, are subjected to a partial discharge source, and the findings are presented in three tables. The major causes of partial discharge, which might vary with each discharge pulse, are pulse width and discharge load amount. These variables are dependent on the source of the partial discharge and are inaccurately calculable. However, investigations and tests suggest that with a proper estimate of the source, approximate values may be taken into consideration.

5.1 PD source location at point A of phase R

Tests were repeated for five distinct sources, and the outcomes were compared in order to strengthen the model's dependability. Figure 9 depicts the coupling capacitor's received and injected partial discharge pulses.

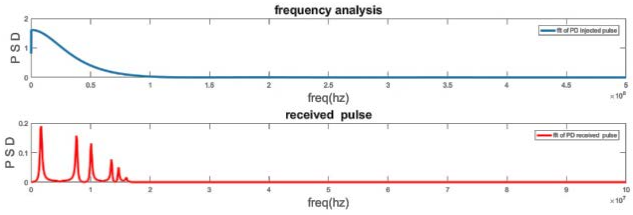

Fig. 9. Partial discharge pulse injected in the source (blue) at point A and the received pulse by the coupling capacitor (red).

Figure 10 displays the partial discharge pulse (blue) that was injected into the source at point A and the coupling capacitor's (red) reception of the pulse together with each pulse's initial peak (The characteristics of the first peak of each pulse are illustrated in the figure).

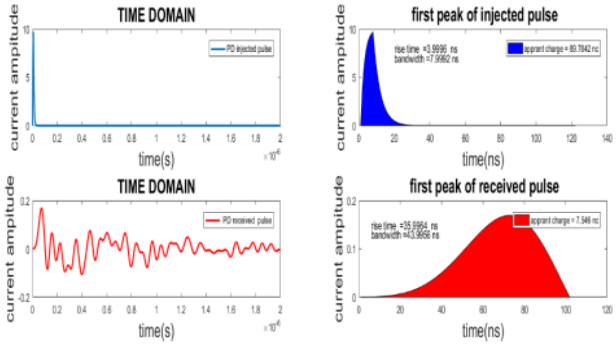

Fig. 10. Partial discharge pulse injected into the source (blue) at point A and the received pulse by the coupling capacitor (red) together with the first peak of each pulse.

5.2 PD source location at point B of phase R

Figures 11 and 12 depict the effects of the partial discharge source replacement in the second model's ninth coil.

Figure 11 displays the partial discharge pulse that was injected into the source at point B (blue) and the coupling capacitor's reception of the pulse (red), along with the initial peak of each pulse (The characteristics of the first peak of each pulse are illustrated in the figure).

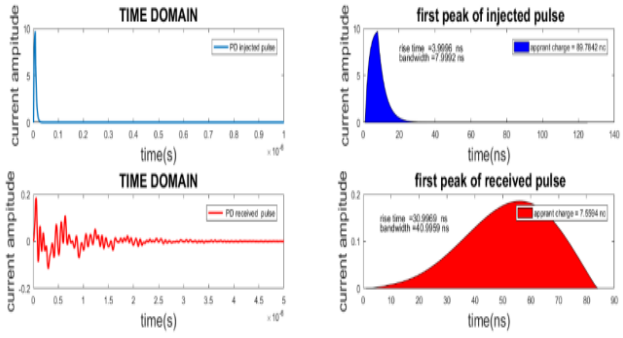

Fig. 11. Partial discharge pulse injected into the source (blue) at point A and the received pulse by the coupling capacitor (red) together with the first peak of each pulse.

Figure 12 displays the partial discharge pulse that was injected into the source at point B (blue) and the coupling capacitor's reception of the pulse (red), along with the initial peak of each pulse (The characteristics of the first peak of each pulse are shown in the figure).

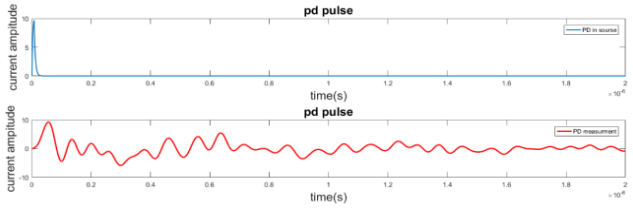

Fig. 12. Partial discharge pulse injected into the source (blue) at point A and the received pulse by the coupling capacitor (red) together with the first peak of each pulse.

5.3 PD source location at point C of phase R

Table 3: Received pulse specifications of experiment 1 for all three models

Model 1	Rise time (ns)	36
	Bandwidth (ns)	44
	Apparent charge (nC)	3.94
Model 2	Rise time (ns)	31
	Bandwidth (ns)	41
	Apparent charge (nC)	3.94
Model 3	Rise time (ns)	25
	Bandwidth (ns)	36
	Apparent charge (nC)	3.91

Figures 13 and 14 show the outcomes of replacing the partial discharge source in the 10th coil of the second model.

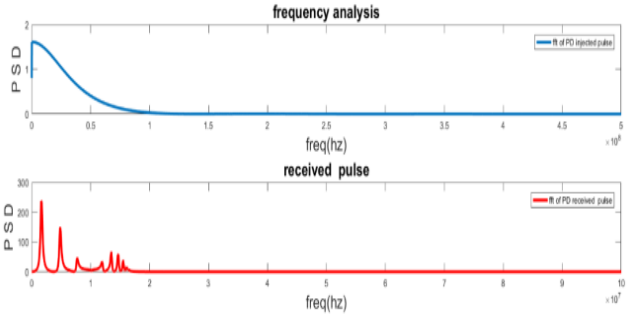

Fig. 13. Partial discharge pulse injected into the source (blue) at point C and the received pulse by the coupling capacitor (red).

Table 4: The results of model 2

Partial discharge source pulse			Received pulse by the capacitor HVCC			Test Number
Rise time (ns)	Band-width (ns)	Apparent charge (nC)	Apparent charge (nC)	Band-width (ns)	Rise time (ns)	
1	5	49.38	3.94	41	31	1
2	6	49.78	4.16	40	31	2
4	8	89.78	7.55	41	31	3
6	9	89.99	7.62	41	31	4
16	34	309.94	20.87	47	35	5

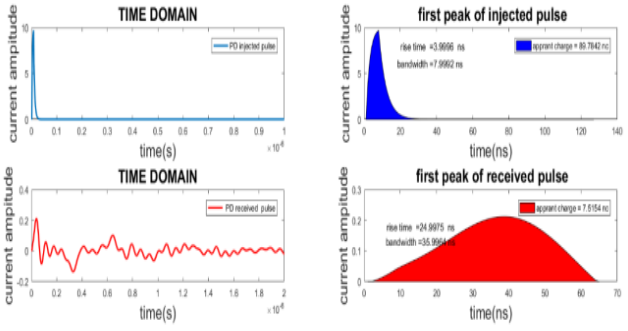

Fig. 14. Partial discharge pulse injected into the source (blue) at point C and the received pulse by the coupling capacitor (red) together with the first peak of each pulse.

5.4 Discussion

Based on Tables 1-3, the source specifications of an experiment for all three models are as follows:

Source load: 49.38 nC
Rising time: 1 ns
Pulse width: 5 ns

Table 4: The results of model 1

Partial discharge source pulse			Received pulse by the capacitor HVCC			Test Number
Rise time (ns)	Band-width (ns)	Apparent charge (nC)	Apparent charge (nC)	Band-width (ns)	Rise time (ns)	
1	3.93	44	36	49.38	5	1
2	4.15	44	35	49.78	6	2
3	7.54	44	36	89.78	8	4
4	7.61	44	36	89.99	9	6
5	21.16	51	40	309.94	34	16

As previously indicated, all three models have the identical source pulse, but the received pulse's pulse rise time and pulse width are different. Lesser amount of rising time and pulse width of the received partial discharge signal, and a partial discharge source that is closer to the motor terminal. In this experiment:

Rising time: 1 ns
Rising pulse time of 8th coil injection source: 36 ns
Rising pulse time of 9th coil injection source: 31 ns
Rising pulse time of 10th coil injection source: 25 ns
Source pulse width Source: 5 ns
Rising pulse time of 8th coil injection source: 44 ns
Rising pulse time of 9th coil injection source: 41 ns
Rising pulse time of 8th coil injection source: 36 ns

6. CONCLUSION

The aim of this research is to identify the best appropriate coupling capacitor-based online PD measuring technique for induction motors. The fault's location was appropriately determined by contrasting the traits of various recorded PD pulses with those of PD applied pulses. Last but not least, the state of the induction motor winding after PD application was examined. The frequency range of the sensor is determined by the capacitor and the measuring impedance collectively. All coupling capacitors have quadrupoles built into the bottom of them, along with over-voltage protection for the safety of the equipment and the users. The frequency range for the quadrupoles is several tens of kilohertz to several hundred megahertz (covering a wide range of frequency). It is possible to synchronize the partial discharge detector with the same signal wire thanks to the specifically constructed quadrupole. Due to the strong magnetic fields present in the testing environment, the virtual grounded signal output shields the signal wires from eddy currents. The process of PD discharge may go quite quickly. Interferences are often not broadband, especially in the high-frequency region, and may frequently be avoided by changing the center frequency. This measurement technique may be used to on-site, online, and commissioning testing. In the study that is being presented, PD on induction motors is tested using a practical manner. Additionally, the PD signal is de-noised using affordable and precise filters. The primary goals of this research are to diagnose the partial discharge occurrence and locate it using the proper tools. In this case, the rise time and pulse width are important variables.

REFERENCES

[1] P. RezaeiBaravati, et al, 2014"Transformer winding modeling based on multi-conductor transmission line model for partial discharge study" Journal of Electrical Engineering and Technology, 9 (1), pp. 154-161.

[2] P. RezaeiBaravati, et al, 2015 "Partial discharge localization based on detailed models of transformer and wavelet transform techniques" Journal of Electrical Engineering and Technology, 10 (3), pp. 1093-1101.

[3] SMH Hosseini, M Vakilian, GB Gharehpetian, 2015 "An improved MTL modeling of transformer winding" International Conference Power System Transients, Lyon, French.

[4] SM Hassan Hosseini, SM Hosseini Bafghi, 2015 "Comparison of high frequency detailed generator models for partial discharge localization" Journal of Electrical Engineering and Technology, 10 (4), pp. 1752-1758.

[5] B. Sheng et al., 2015 "A novel on-line cable PD localization method based on the cable transfer function and detected PD pulse rise-time," in IEEE Transactions on Dielectrics and Electrical Insulation, vol. 22, no. 4, pp. 2087-2096.

[6] E. T. Iorkyase, C. Tachtatzis, I. A. Glover and R. C. Atkinson, 2019 "RF-based location of partial discharge sources using received signal features," in High Voltage, vol. 4, no. 1, pp. 28-32.

[7] Luo, Yuanlin; Li, Zhaohui; Wang, Hong. 2017. "A Review of Online Partial Discharge Measurement of Large Generators." Energies 10, no. 11: 1694.

[8] Romano, Pietro; Imburgia, Antonino; Ala, Guido. 2019. "Partial Discharge Detection Using a Spherical Electromagnetic Sensor." Sensors 19, no. 5: 1014.

[9] H. Karami, G. B. Gharehpetian, Y. Norouzi and M. A. Hejazi, 2018 "Experimental Study on Elimination of Partial Discharge Effect on Detection of Radial Deformation of High Voltage Transformer Winding Using Electromagnetic Waves," 2018 IEEE International Conference on Environment and Electrical Engineering and 2018 IEEE Industrial and Commercial Power Systems Europe (EEEIC / I&CPS Europe), Palermo, pp. 1-5.

[10] Wadi, Ali, Wasim M. F. Al-Masri, Wisal Siyam, Mamoun F. Abdel-Hafez and Ayman El-Hag. 2018 “Accurate Estimation of Partial Discharge Location using Maximum Likelihood.” IEEE Sensors Letters 2 (2018): 1-4.

[11] Dukanac, Djordje, 2018, Application of UHF method for partial discharge source location in power transformers. IEEE Transactions on Dielectrics and Electrical Insulation. 25. 2266-2278. 10.1109/TDEI.2018.006996.

[12] Gao, Chaofei, Wei Wang, Shu Song, Shaojin Wang, Lei Yu and Y. F. Wang., 2018 “Localization of partial discharge in transformer oil using Fabry-Pérot optical fibre sensor array.” IEEE Transactions on Dielectrics and Electrical Insulation 25, pp 2279-2286.

[13] Zhang, Tian-Ting, Gui-ping Zhou and Shunjiang Wang. 2018, “Application of Distributed Partial Discharge Detection Technique Synchronized with AC Withstand Voltage Test of High Voltage Cable.” 2018 2nd IEEE Conference on Energy Internet and Energy System Integration (EI2): pp 1-5.

[14] Hu, Yue, Zijing Zeng, Jiangting Liu, Jianwen Wang and Weidong Zhang, 2018 “Design of a Distributed UHF Sensor Array System for PD Detection and Location in Substation.” 2018 Conference on Precision Electromagnetic Measurements (CPEM 2018), pp 1-3.

[15] G. Callender, P. Rapisarda and P. L. Lewin, 2017 "Improving models of partial discharge activity using simulation," 2017 IEEE Electrical Insulation Conference (EIC), Baltimore, MD, pp. 392-395.

[16] G. Callender, P. L. Lewin and G. C. Montanari, 2018 "Simulation of Partial Discharge under Impulse Voltage Waveforms," 2018 IEEE 2nd International Conference on Dielectrics (ICD), Budapest, pp. 1-4.

[17] Chen, Mu-Kuen & Cheng, Chao-Yuan & Chen, Jeng. 2016, Partial discharge detection of the 3.3-kV motor by coil: Partial Discharge, Motor, Coil Sensor. International Transactions on Electrical Energy Systems. 27. 10.1002/etep.2241.

[18] Wang, Meng-Hui, Shiue-Der Lu and Meng-Ju Hsieh. 2018 “Application of extension neural network algorithm and chaos synchronization detection method to partial discharge diagnosis of power capacitor.” (2018).

[19] Jitjing, Pinit & Suwanasri, Thanapong & Suwanasri, Cattareeya. 2016, The Design of Electrode for Partial Discharge Location Simulation in Oil Insulated Power Transformer and the Application of AE Method. Procedia Computer Science. 86. 289-292. 10.1016/j.procs.2016.05.074.

[20] W. M. F. Al-Masri, M. F. Abdel-Hafez and A. H. El-Hag, "Toward High-Accuracy Estimation of Partial Discharge Location," in IEEE Transactions on Instrumentation and Measurement, vol. 65, no. 9, pp. 2145-2153.

[21] B. Wang, M. Dong, M. Ren, Z. Wu and A. Ma, 2016 "Partial discharge ultrasonic localization simulation based on double helix ultrasonic sensor array," 2018 12th International Conference on the Properties and Applications of Dielectric Materials (ICPADM), Xi'an, 2018, pp. 136-139.

[22] Iorkyase, Ephraim, Christos Tachtatzis, Pavlos I. Lazaridis, Ian A. Glover and Robert C. Atkinson. 2017“Radiolocation of partial discharge sources: a support vector regression approach”.

[23] Z. Lu et al., 2015 "Diagnosis and analysis for a typical defect of partial discharge in GIS," 2015 5th International Conference on Electric Utility Deregulation and Restructuring and Power Technologies (DRPT), Changsha, pp. 1612-1616.

[24] Amin, Emran M. and Nemai C. Karmakar.2016 “A Passive RF Sensor for Detecting Simultaneous Partial Discharge Signals Using Time-Frequency Analysis.” IEEE Sensors Journal 16, pp 2339-2348.

[25] Yu Ming, S. Birlasekaran and S. S. Choi,2005 "Simulation of partial discharge propagation in the power network," in IEEE Transactions on Energy Conversion, vol. 20, no. 3, pp. 644-653.